Thermal Dissociation of Streptavidin Homotetramer in the Gas Phase.

Subunit Loss versus Backbone Fragmentation

Elena N. Kitova, Igor Sinelnikov, Lu Deng and John S. Klassen*

Department of Chemistry, University of Alberta, Edmonton, Alberta, Canada T6G 2G2

Abstract

The results of time-resolved blackbody infrared radiative dissociation experiments performed on gaseous protonated ions, at charge states +15, +16 and +17, of the homotetramer streptavidin (S_4) are reported. Evidence is found for three dissociation pathways involving (*i*) the loss of a single subunit, (*ii*) covalent cleavage of the backbone of one of the subunits and ejection of the resultant b_{21}^{2+} ion (followed by loss of complementary y_{106} ions), and (*iii*) the direct loss of one or more water molecules. The contribution of the different dissociation channels was found to be dependent on temperature, with the loss of subunit dominating at higher reaction temperatures and backbone fragmentation dominating at lower temperatures, and reaction times, with longer times favouring covalent fragmentation. Analysis of the dissociation kinetics and the influence of reaction time on the relative abundance of product ions indicate that backbone fragmentation and subunit loss are not produced via parallel pathways from a single reactant. Instead, the results suggest the presence of multiple, non-interconverting structures, which contribute differentially to the backbone fragmentation and subunit loss pathways. The results of molecular dynamics simulations performed on S_4^{+16} ions with different charge configurations suggest that unfolding of the N-terminus of the subunit may be associated with the backbone fragmentation pathway.

1. Introduction

Electrospray ionization mass spectrometry (ESI-MS) is an important tool for characterizing noncovalent protein assemblies and is increasingly used to establish subunit composition and topology [1-5]. These structural insights are often obtained by heating (activating) protein complexes in the gas phase in order to induce structural changes, usually dissociation reactions. Activation of the gas phase ions of protein complexes is most commonly achieved through energetic collisions with neutral gases (collision-induced dissociation, CID) [6-8]. However, other activation methods can also be used, such as surface-induced dissociation (SID) [9], the blackbody infrared radiative dissociation (BIRD) technique, which involves absorption of blackbody radiation in a near collision-free environment [10-14], or electron mediated methods, such as electron capture dissociation (ECD) [15].

The loss of one or more subunits from the protein complex is usually the major dissociation pathway observed with CID, SID and BIRD. With CID, which is a relatively slow heating method (on the μs timescale), the ejected subunit typically retains a disproportionately large fraction (based on mass) of the total charge of the complex [6-8,16-18]. Similar observations have been made using BIRD, for which activation occurs on a much longer timescale (~s) compared to CID [10-14]. It is generally accepted that activation of the gaseous complex ion results in the unfolding of at least one of the subunits [7,8,19,20]. The resulting increase in surface area of the unfolding subunit promotes charge (usually proton) transfer, which decreases the total Coulombic repulsion in the complex ion [13,21,22]. In the case of SID, which involves significantly shorter activation timescales (~ns) and high collision energies, the subunit loss reaction is typically more charge symmetric in nature [9,18]. The difference in charge distributions

observed in SID and CID has been attributed to faster subunit loss kinetics in SID, which dominates over the unfolding/charge transfer processes [18].

While subunit loss represents the most common pathway for the dissociation of protein complexes in the gas phase, other dissociation pathways have been reported. In some instances the loss of intact subunit multimers is observed [23-25]. There have also been a limited number of reports of backbone fragmentation reactions competing with subunit loss from the intact protein complex. For example, McLuckey and coworkers reported on CID of the heterodimer complex of trypsin and bovine pancreatic trypsin inhibitor (BPTI) [26]. At the lowest charge states investigated they noted the loss of (unidentified) neutrals as the dominant dissociation pathway. They also observed the ejection of a cation, which was tentatively assigned as the b_2 ion corresponding to backbone fragmentation of BPTI. It was suggested that the cleavage site was related to an absence of intermolecular interactions between the N-terminus of BPTI and trypsin in the gas phase complex. Similarly, Wysocki and co-workers found that CID of the homopentamer of serum amyloid P (SAP) component resulted in covalent fragmentation of the protein backbone, producing b-type ions, in addition to the subunit loss [18]. In contrast, SID of SAP at the same charge state produced exclusively intact monomers and dimers. It was suggested that proton transfer to the unfolding subunit, which occurs during CID, but not SID, is necessary for covalent cleavage to occur. More recently, Robinson and co-workers observed covalent fragmentation, resulting in the production of y-type ions, in CID of the homotetrameric complex of human transthyretin [17]. Interestingly, while subunit loss occurred at all charge states investigated, covalent bond fragmentation was observed only for the lowest charge states. This finding led to the

suggestion that the covalent fragmentation pathways are not governed only by subunit unfolding and proton migration.

Here, we describe the results of time-resolved BIRD experiments performed on gaseous protonated ions of streptavidin. Streptavidin is a homotetrameric protein complex (S_4) that is isolated from *Streptomyces avidinii*. Streptavidin has been the focus of previous gas phase dissociation studies [6,13]. Smith and co-workers applied sustained off-resonance irradiation (SORI)-CID to the protonated S_4 ion at charge state +14. Dissociation produced exclusively the S^{+7} and S_3^{+7} and S^{+6} and S_3^{+8} product ion pairs [6]. More recently, time-resolved BIRD experiments were performed on the protonated S_4 ions at charge states +14, +15 and +16 [13]. At relatively short reaction times, the major dissociation pathway, independent of temperature, was the loss of a single subunit carrying nearly 50% of the total charge. The first-order kinetic plots were found to be non-linear, a finding attributed to the presence of multiple, non-interconverting structures with distinct dissociation rate constants or thermally-induced changes in the conformation of the complex.

The present work, which is an extension of the earlier BIRD study [13], examines the dissociation of protonated S_4 ions, at the +15, +16, +17 charge states, composed of a recombinant, truncated form of streptavidin, which is produced predominantly as a single isoform. The homogeneity of the protein facilitated the identification of new dissociation pathways - backbone fragmentation and water loss – that were not evident in the previous CID or BIRD studies. The influence of reaction time, temperature and reactant ion charge state on these pathways was assessed. Molecular dynamics (MD) simulations, which have been shown previously to be useful for probing the structures of protein complexes in the gas phase and their dissociation pathways [21,27-29], were used to investigate the

influence of the charge distribution on the extent of unfolding of the N-terminus of the subunit.

Experimental

A recombinant, truncated form (containing residues 13-139) of wild type streptavidin (monomer MW 13 271.5 Da) was used in this study. The plasmid was generously provided by Prof. P. Stayton (University of Washington). The protein was expressed in *E. coli* and purified using procedures described elsewhere [30]. The solution of purified S_4 was exchanged directly into 200 mM aqueous ammonium acetate using an Amicon microconcentrator with a MW cut-off of 10 kDa and lyophilized. Stock solution of S_4 (100 μM) was prepared by dissolving a known amount of lyophilized streptavidin into 200 mM ammonium acetate and stored at -20 °C until needed. ESI solutions were prepared by thawing the stock solution at room temperature and diluting an aliquot with aqueous ammonium acetate (10 mM) to achieve a S_4 concentration of 10 μM.

All experiments were performed using an ApexII 9.4T Fourier-transform ion cyclotron resonance mass spectrometer (Bruker, Billerica, MA). Nanoflow ESI (nanoESI) was performed using borosilicate tubes (1.0 mm o.d., 0.68 mm i.d.), pulled to ~5 μm o.d. at one end using a P-97 micropipette puller (Sutter Instruments, Novato, CA). The electric field required to spray the solution in positive ion mode was established by applying a voltage of 0.8 – 1.1 kV to a platinum wire inserted inside the glass tip. The solution flow rate was ~20 nL min^{-1}. To shift the S_4^{n+} ions to higher charge states, nanoESI was performed using a custom built device that directs a high velocity flow of dry air at the end of the ESI tip [31]. Details of the instrumental and experimental conditions used for the BIRD measurements can be found elsewhere [32,33].

Molecular dynamics simulations

MD simulations were carried out using NAMD 2.9 [34] with the Amber03 force field [35] under vacuum. The initial geometry of the S_4 complex was obtained from the crystal structure of streptavidin (PDB ID: 1SWB) [36]. Each of the subunits (containing residues 16-135 for subunit A, residues 16-133 for subunits B, C and D) was extended to have the same length as the truncated form (containing residues 13-139) of streptavidin that was used experimentally. This was done by aligning each subunit against the subunit C of the crystal structure for streptavidin mutant Ser27Ala (PDB ID: 1N9M) [37] using the DALI server [38], and grafting the extended residues onto each subunit of the tetramer.

Ions of the S_4 complex at the +16 charge state at five different charge distributions (Table 1) were chosen for investigation. Topology and coordinate files for the simulations of each charge distributions were generated using the xleap module of the AmberTools (version 11) [39]. It was necessary to develop charges and parameters for the neutral forms of Arg and C-terminal Ser as well as protonated forms of Ala, Asn and Tyr. The charge parameters for these non-standard residues were parameterized using the RESP ESP charge Derive server (RED Server) [40,41], using Gaussian C.01 [42] and enforcing net charge across the residue. The MD integration time step was 1 fs; bonds involving hydrogen atoms were constrained with SHAKE. Following 1000 steps of minimization, the system was gradually heated to 500K within 250000 steps. The temperature was then held constant at 500K and 2.5 ns of dynamics were performed. Trajectory analysis, performed using the Visual Molecular Dynamics package [43], was carried out to establish the C_α root mean square deviation (RMSD). The first 1.5 ns of dynamics were needed to fully equilibrate the system, as judged by RMSD. The subsequent 1.0 ns of production were used in the analysis.

Results and discussion

Shown in Figure 1 are ESI mass spectra acquired in positive ion mode, with and without the use of the gas-assisted nanoESI device, for an aqueous ammonium acetate solution of 10 μM S_4. When using the gas-assisted nanoESI device, the major protein ions detected correspond to protonated S_4 (measured MW 53 085 ± 1 Da, theoretical MW 53 086 Da) i.e., S_4^{n+}, at charge states n = 15 to 18 (Figure 1a). In contrast, when using normal nanoESI, S_4^{n+} ions were detected at charge states n = 14 to 17. The shift of the charge state distribution to higher values is, presumably, due to the dilution of agents such as NH_3 and H_2O that can effect proton transfer and remove charge from the protein ions. Also observed in the mass spectrum is a series of low abundance ions that correspond to a species with a MW of 53 219 ± 1 Da. This species is assumed to be a streptavidin tetramer that contains three copies of the expected natural core streptavidin subunit and one isoform of streptavidin, which has an additional N-terminal Met residue, i.e., (S_4 + Met). The theoretical MW of the proposed tetrameric streptavidin complex is 53 218 Da [44].

Time-resolved BIRD experiments were performed on the S_4^{+15}, S_4^{+16} and S_4^{+17} ions, at temperatures ranging from 131 to 161 ^oC. Shown in Figure 2 are mass spectra acquired for the S_4^{+16} ion, following isolation (Figure 2a), and after 2 s and 5 s at 161 ^oC (Figures 2b,c). At this temperature, the major dissociation pathway corresponds to the loss of a subunit, i.e., S^{n+} with n = 7 – 9, and formation of the complementary S_3^{n+} ions, at n = 7 - 9. In addition to the ions produced from the subunit loss pathway, a doubly charged ion at m/z ~1083, and ions at m/z 1585 and 1849 were detected. The m/z 1083 ion corresponds to the $(b_{21} - H_2O)^{2+}$ ion, which is formed by cleavage of the Ala21-Gly22

amide linkage (and the loss of water), while the m/z 1585 and 1849 ions correspond to the truncated subunit, which are nominally the y_{106}^{7+} and y_{106}^{6+} ions. Also observed in the BIRD mass spectra is an ion at m/z 3637, which is the truncated S_4^{+14} ion produced by the loss of b_{21}^{2+}, i.e., $(S_4 - b_{21})^{+14} \equiv (S_3y_{106})^{+14}$. A third dissociation pathway involves the loss of one and, possibly, more water molecules directly from the S_4^{+16} ion. The appearance of the low abundance $(S_3y_{106} - H_2O)^{+14}$ and $(S - H_2O)^{+9}$ ions indicates that the $(S_4 - H_2O)^{+16}$ ion dissociates in a manner similar to the S_4^{+16} ion. Taken together, these results suggest that the b_{21}^{2+} ion, which subsequently loses H_2O to give the $(b_{21} - H_2O)^{2+}$ ion, is lost directly from the S_4^{+16} ion, followed by the loss of the truncated subunit (y_{106}), which is ejected at the +6 and +7 charge states. A small amount of the proton transfer product, the S_4^{+15} ion, was also detected.

Shown in Figure 3 are representative BIRD mass spectra acquired for the S_4^{+16} ion at 151, 141 and 131 ^{o}C. It can be seen that the BIRD results obtained at 151 ^{o}C are qualitatively similar to those at 161 ^{o}C, with evidence for pathways involving subunit loss, covalent fragmentation and water loss. At 141 and 131 ^{o}C, the $(S_3y_{106})^{+14}$ ion is the major product ion observed; ions corresponding to the water loss are also detected. However, the y_{106}^{6+} and y_{106}^{7+} ions are absent from the mass spectra. This result indicates that the $(S_3y_{106})^{+14}$ ion is kinetically more stable than the S_4^{+16} ion, and resists dissociation (except for the loss of water) at these temperatures. This finding can be explained by the lower Coulombic repulsion between S_3 and the truncated subunit. These results also suggest that the activation energy (E_a) for the backbone fragmentation pathway, leading to the $(S_3y_{106})^{+14}$ ion, is lower than that for intact subunit ejection.

Representative BIRD mass spectra acquired for the S_4^{+15} and S_4^{+17} ions are shown in Figures 4 and 5. Qualitatively, the BIRD results for these ions are similar to those

described for the S_4^{+16} ion, with evidence for subunit ejection, backbone fragmentation and water loss. As was found for S_4^{+16} ion, the relative contribution of the backbone cleavage pathway to the BIRD mass spectra for the S_4^{+15} and S_4^{+17} ions was more significant at lower reaction temperatures. The $(S_3y_{106})^{+15}$ ion produced the expected y_{106}^{n+} ions (at n = 6 - 8) at 161 and 151 ^oC but not at lower temperatures, similar to what was found for the $(S_3y_{106})^{+14}$ ion. In contrast, the $(S_3y_{106})^{+13}$ ion was found to be kinetically stable at the temperatures investigated and no y_{106}^{n+} ions were detected.

The BIRD mass spectra reveal that there are multiple dissociation channels accessible to the S_4^{n+} ions. An obvious question to ask is whether these represent parallel pathways originating from a single reactant. Shown in Figure 6a are plots of the natural logarithm of the normalized abundance of the S_4^{+16} ion versus time measured at the four reaction temperatures considered. It can be seen, particularly at the lower temperatures investigated, that the plots are non-linear. Kinetic plots obtained for charge sates +15 and +17 are also non-linear (data not shown). Plotted in Figure 6b is the ratio ($R_{C/S}$) of the abundances of the unique products produced by backbone fragmentation ($(S_3y_{106})^{+14}$, y_{106}^{6+} and y_{106}^{7+} ions) and subunit loss (S^{+7}, S^{+8} and S^{+9}) versus the fraction of S_4^{+16} that has reacted, measured at 161, 151 and 141 ^oC. It can be seen that $R_{C/S}$ increases with the extent of dissociation of the reactant ion, indicating that the backbone fragmentation pathway becomes more prominent as the reaction proceeds. Qualitatively similar results were obtained for the S_4^{+15} and S_4^{+17} (data not shown). These findings rule out the possibility of parallel pathways involving a single reactant and, instead, suggest the presence of multiple non-interconverting structures or the occurrence of structural changes to the reactant ion, on the timescale of the reaction, which influence the rate of dissociation. However, an analysis of the average charge states of the S^{n+}, S_3^{n+} and y_{106}^{n+}

ions produced from the three S_4^{n+} ions fails to reveal any time and temperature dependence. Assuming that the charge states of the product ions are sensitive to their structure and, in particular, surface area [17,45], this result would seem to argue against structural changes taking place over the course of the reaction.

Taken together the BIRD results indicate that lower temperatures and longer reaction times promote backbone fragmentation. As discussed above, the influence of temperature can be explained in terms of a lower E_a for backbone fragmentation compared to that for subunit loss. This is consistent with the E_a values reported previously for the fragmentation of small proteins and peptides and subunit loss from mulitprotein complexes in the gas phase [11,13,46]. The influence of reaction time on the different pathways is explained by the presence of multiple, non-interconverting S_4^{n+} structures, which contribute differentially to the dissociation pathways. Overall, the kinetic stability of the S_4^{n+} ions decreases with increasing charge state, a finding that can be explained in terms of the destabilizing effect of Coulombic repulsion within the S_4^{n+} ions. However, the backbone cleavage pathway was not found to be strongly dependent on the charge state of the S_4^{n+} ion.

That backbone fragmentation of the S_4^{n+} ions occurs at only one site, the Ala21-Gly22 amide linkage, is intriguing and suggests that the E_a for cleavage at this particular linkage is small compared to the other amide bonds. It is not obvious from the primary structure why this particular site is unusually labile, although it has been shown that backbone cleavage on the N-terminal side of Gly residues is commonly observed in CID of protonated peptides [18,47]. An analysis of the crystal structure of S_4 indicates that the residues that make up the b_{21} fragment are involved in two β-strands, with the Ala21 residue located at the end of the second β-strand. Based on the arguments advanced by

McLuckey and co-workers [26], the selectivity of the cleavage site may be related to the unfolding of the N-terminal portion of the subunit, which promotes protonation of Ala21.

In an effort to gain more insight into the selectivity of the fragmentation reaction, MD simulations were performed on S_4^{+16} ions with five different charge configurations (Table 1). For four of the configurations considered, the charges were distributed asymmetrically between subunits: seven charges were placed on one subunit (subunit A) and nine charges were evenly distributed between remaining three subunits. In each case, the N-terminus, as well as Arg47, Arg72, Lys109 and Lys120 were protonated; the position of the remaining charges was varied: Asn11 and Arg41 (configuration 16_1), Ala21 and Arg41 (16_2), Tyr31 and Arg41 (16_3), and Arg41 and Arg 91 (16_4). A symmetric charge configuration was also considered (16_5), in which the charges were located on the N-terminus, Arg41, Arg47 and Lys120 of each of the subunits.

Shown in Figure 7 are representative MD snapshots of the S_4^{+16} ions with the different charge configurations, as well as the crystal structure of S_4. The MD results indicate that the location of the charges influences the structure of the subunits. Overall, the structures of the S_4^{+16} ions associated with the symmetric charge configuration (16_5) and two of the asymmetric charge configurations (16_1 and 16_4) were found to resemble the crystal structure. However, there are significant structural differences in subunit A for the charge configurations 16_2 (RMSD ~7 Å, calculated for subunit A) and 16_3 (RMSD ~15 Å, calculated for subunit A). In the case of 16_3, the four β-strands comprising residues 1 – 48 of subunit A still exist but have shifted greatly from their original positions (as seen in the crystal structure). However, in the case of configuration 16_2, protonation of Ala21 – the site of backbone cleavage – promotes complete unfolding of the first two β-strands of the N-terminal region of subunit A (RMSD >9 Å,

calculated for residues 1 – 21). While the results of the MD simulations do not provide a conclusive explanation for the cleavage site specificity, they do raise the possibility that thermal unfolding of the N-terminal region of one of the subunits promotes protonation of the Ala21 residue, which may in turn promote amide bond cleavage.

Conclusions

In summary, the results of time-resolved BIRD experiments performed on gaseous protonated S_4^{+15}, S_4^{+16} and S_4^{+17} ions reveal three different primary dissociation pathways: the loss of a subunit, covalent cleavage of the backbone and concomitant ejection of the resultant b_{21}^{2+} ion, and the direct loss of water molecules. The contribution of the different dissociation channels was found to be dependent on temperature, with the loss of subunit dominating at the higher temperatures and backbone fragmentation dominating at lower temperatures, and reaction time, with longer times favouring covalent fragmentation. Analysis of the relative abundance of product ions measured as a function of the extent of reaction reveals that backbone fragmentation and subunit loss are not produced via parallel pathways from a single reactant. Instead, the results are consistent with the presence of multiple non-interconverting structures, which contribute differentially to the dissociation pathways. The results of MD simulations performed on S_4^{+16} ions with different charge configurations suggest that unfolding of the N-terminal region of the subunit may be associated with the formation in the b_{21}^{2+} ion.

Acknowledgements

The authors acknowledge the Natural Sciences and Engineering Research Council of Canada and the Alberta Glycomics Centre for funding, A. Broom (University of Waterloo) for technical assistance and Professor P. Stayton (University of Washington)

for generously providing the plasmid for streptavidin. The MD simulations were made possible by the facilities of the Shared Hierarchical Academic Research Computing Network (SHARCNET: www.sharcnet.ca) and Compute/Calcul Canada.

References

[1] J.A. Loo, Electrospray ionization mass spectrometry: a technology for studying noncovalent macromolecular complexes. Int. J. Mass Spectrom. 200 (2000) 175-186

[2] J.L.P. Benesch, C.V. Robinson, Mass spectrometry of macromolecular assemblies: preservation and dissociation. Curr. Opin. Struct. Biol. 16 (2006) 245-251

[3] N.P. Barrera, C.V. Robinson, Advances in the mass spectrometry of membrane proteins: from individual proteins to intact complexes. Annu. Rev. Biochem. 80 (2011) 247-271.

[4] C. Uetrecht, A.J. Heck, Modern biomolecular mass spectrometry and its role in studying virus structure, dynamics, and assembly. Angew. Chemie Int. Ed. 50 (2011) 8248–8262

[5] R.H.H. van den Heuvel, A.J.R. Heck, Native protein mass spectrometry: from intact oligomers to functional machineries. Curr. Opin. Chem. Biol. 8 (2004) 519–526

[6] B.L. Schwartz, J.E. Bruce, G.A. Anderson, S.A. Hofstadler, A.L. Rockwood, A. Chilkoti, P.S. Stayton, R.D. Smith, Dissociation of tetrameric ions of noncovalent streptavidin complexes formed by electrospray ionization. J. Am. Soc. Mass Spectrom. 6 (1995) 459–465

[7] J.L.P. Benesch, B.T. Ruotolo, D.A. Simmons, C.V. Robinson, Protein complexes in the gas phase: technology for structural genomics and proteomics. Chem. Rev. 107 (2007) 3544-3567

[8] J.C. Jurchen, E.R. Williams, Origin of asymmetric charge partitioning in the dissociation of gas-phase protein homodimers. J. Am. Chem. Soc. 125 (2003) 2817-2826

[9] C.M. Jones, R.L. Beardsley, A.S. Galhena, S. Dagan, G.L Cheng, V.H. Wysocki, Gas-phase dissociation energetics of noncovalent protein complexes probed by surface-induced dissociation mass spectrometry. J. Am. Chem. Soc. 128 (2006) 15044-15045

[10] R.C. Dunbar, T.B. McMahon, Activation of unimolecular reactions by ambient blackbody radiation. Science 279 (1998) 194-197

[11] N. Felitsyn, E.N. Kitova, J.S. Klassen, Thermal decomposition of a gaseous multiprotein complex studied by blackbody infrared radiative dissociation. Investigating the origin of the asymmetric dissociation behavior. Anal. Chem. 73 (2001) 4647–4661

[12] N. Felitsyn, E.N. Kitova, J.S. Klassen, Thermal dissociation of the protein homodimer ecotin in the gas phase. J. Am. Soc. Mass Spectrom. 13 (2002) 1432–1442

[13] I. Sinelnikov, E.N. Kitova, J.S. Klassen, Influence of Coulombic repulsion on the dissociation pathways and energetics of multiprotein complexes in the gas phase. J. Am. Soc. Mass Spectrom. 18 (2007) 617–631

[14] I. Sinelnikov, E.N. Kitova, J.S. Klassen, Effects of single amino acid substitution on the dissociation of multiply charged multiprotein complexes in the gas phase. J. Am. Soc. Mass Spectrom. 18 (2007) 688–692

[15] R.B.J. Geels, S.M. van der Vies, A.J.R. Heck, R.M.A. Heeren, Electron capture dissociation as structural probe for noncovalent gas-phase protein assemblies. Anal. Chem. 78 (2006) 7191-7196

[16] K.J. Light-Wahl, B.L. Schwartz, R.D. Smith, Observation of the noncovalent quaternary associations of proteins by electrospray ionization mass spectrometry. J. Am. Chem. Soc. 116 (1994) 5271-5278

[17] K. Pagel, S.-J. Hyung, B.T. Ruotolo, C.V. Robinson, Alternate dissociation pathways identified in charge-reduced protein complex ions, Anal. Chem. 82 (2010) 5363-5372

[18] V.H. Wysocki, C.M. Jones, A.S. Galhena, A.E. Blackwell, Surface-induced dissociation shows potential to be more informative than collision-induced dissociation for structural studies of large systems, J. Am. Soc. Mass Spectrom. 19 (2008) 903–913

[19] B.T. Ruotolo, S.-J. Hyung, P.M. Robinson, K. Giless, R.H. Bateman, C.V. Robinson, Ion mobility–mass spectrometry reveals long-lived, unfolded intermediates in the dissociation of protein complexes. Angew. Chem. Int. Ed. 46, 2007, 8001-8004

[20] J.L.P. Benesch, Collisional activation of protein complexes: picking up the pieces. J. Am. Soc. Mass Spectrom. 20 (2009) 341–348

[21] S.N. Wanasundara, M. Thachuk, Theoretical investigations of the dissociation of charged protein complexes in the gas phase. J. Am. Soc. Mass Spectrom. 18 (2007) 2242–2253

[22] J.L.P. Benesch, J.A. Aquilina, B.T. Ruotolo, F. Sobott, C.V. Robinson, Tandem mass spectrometry reveals the quaternary organization of macromolecular assemblies. Chem. Biol. 13, 2006, 597-605

[23] A.J. Aquilina, The major toxin from the Australian Common Brown Snake is a hexamer with unusual gas-phase dissociation properties. Proteins 75 (2009) 478-485

[24] R.H. van den Heuvel, E. van Duijn, H. Mazon, S.A. Synowsky, K. Lorenzen, C. Versluis, S.J. Brouns, D. Langridge, J. van der Oost, J. Hoyes, A.J. Heck, Improving the performance of a quadrupole time-of-flight instrument for macromolecular mass spectrometry. Anal. Chem. 78 (2006) 7473–7483

[25] E.B. Erba, B.T. Ruotolo, D. Barsky, C.V. Robinson, Ion mobility-mass spectrometry reveals the influence of subunit packing and charge on the dissociation of multiprotein complexes. Anal. Chem. 82 (2010) 9702–9710

[26] S.J. Pitteri, P.A. Chrisman, E.R. Badmanb, S.A. McLuckey, Charge-state dependent dissociation of a trypsin/inhibitor complex via ion trap collisional activation, Int. J. Mass Spectrom. 253 (2006) 147–155

[27] S.N. Wanasundara, M. Thachuk, Free energy barrier estimation for the dissociation of charged protein complexes in the gas phase. J. Phys. Chem. A 113 (2009) 3814–3821

[28] S.N. Wanasundara, M. Thachuk, Toward an improved understanding of the dissociation mechanism of gas phase protein complexes. J. Phys. Chem. B 114 (2010) 11646–11653

[29] Z. Hall, A. Politis, M.F. Bush, L.J. Smith, C.V. Robinson, Charge-state dependent compaction and dissociation of protein complexes: insights from ion mobility and molecular dynamics. J. Am. Chem. Soc. 134 (2012) 3429-3438

[30] A. Chilkoti, P.H. Tan, P.S. Stayton, Site-directed mutagenesis studies of the high-affinity streptavidin-biotin complex - contributions of tryptophan residue-79, residue-108, and residue-120. Proc. Natl. Acad. Sci. U.S.A. 92 (1995) 1754-1758

[31] D. Bagal, E.N. Kitova, L. Liu, A. El-Hawiet, P.D. Schnier, J.S. Klassen, Gas phase stabilization of noncovalent protein complexes formed by electrospray ionization. Anal. Chem. 81 (2009) 7801–7806

[32] E.N. Kitova, M. Seo, P.-N. Roy, J.S. Klassen, Elucidating the intermolecular interactions within a desolvated protein-ligand complex. An experimental and computational study. J. Am. Chem. Soc. 130 (2008) 1214-1226

[33] L. Liu, D. Bagal, E.N. Kitova, P.D. Schnier, J.S. Klassen, Hydrophobic protein-ligand interactions preserved in the gas phase. J. Am. Chem. Soc. 131 (2009) 15980-15981

[34] J.C. Phillips, R. Braun, W. Wang, J. Gumbart, E. Tajkhorshid, E. Villa, C. Chipot, R.D. Skeel, L. Kale, K. Schulten, Scalable molecular dynamics with NAMD. J. Comput. Chem. 26(2005) 1781- 1802

[35] Y. Duan, C. Wu, S. Chowdhury, M.C. Lee, G. Xiong, W. Zhang, R. Yang, P. Cieplak, R. Luo, T. Lee, J. Caldwell, J. Wang, P. Kollman, A point-charge force field for molecular mechanics simulations of proteins based on condensed-phase quantum mechanical calculations. J. Comput. Chem. 24 (2003) 1999-2012

[36] R.E. Stenkamp, I.L. Trong, L. Klumb, P.S. Stayton, S. Freitag, Structural studies of the streptavidin binding loop. Protein Sci. 6 (1997) 1157-1166

[37] N. Ramasubbu, C. Ragunath, P.J. Mishra, L.M. Thomas, G. Gyémánt, L. Kandra, Human salivary α-amylase Trp58 situated at subsite −2 is critical for enzyme activity. Eur. J. Biochem. 271 (2004) 2517-2529

[38] L. Holm, P. Rosenström, Dali server: conservation mapping in 3D. Nucleic Acids Res. 38 (2010) W545-W549

[39] J. Wang, W. Wang, P.A. Kollman, D.A. Case, Automatic atom type and bond type perception in molecular mechanical calculations. J. Mol. Graphics Modell. 25 (2006) 247-260

[40] E. Vanquelef, S. Simon, G. Marquant, E. Garcia, G. Klimerak, J.C. Delepine, P. Cieplak, F.-Y. Dupradeau, R.E.D. Server: a web service for deriving RESP and ESP charges and building force field libraries for new molecules and molecular fragments. Nucleic Acids Res. 39 (2011) W511-W517

[41] F.-Y. Dupradeau, A. Pigache, T. Zaffran, C. Savineau, R. Lelong, N. Grivel, D. Lelong, W. Rosanski, P. Cieplak, The R.E.D. tools: advances in RESP and ESP charge derivation and force field library building. Phys. Chem. Chem. Phys. 12 (2010) 7821-7839

[42] M.J. Frish, Gaussian 09; Gaussian, Inc., Wallingford CT, 2009

[43] J.C. Phillips, R. Braun, W. Wang, J. Gumbart, E. Tajkhorshid, E. Villa, C. Chipot, R.D. Skeel, L. Kalé, K. Schulten, Scalable molecular dynamics with NAMD. J. Comput. Chem. 26 (2005) 1781-1802

[44] T. Sano, M.W. Pandori, X. Chen, C.L. Smith, C.R. Cantor, Recombinant core streptavidins. J. Biol. Chem. 270 (1995) 28204-28209

[45] I.A. Kaltashov, A. Mohimen, Estimates of protein surface areas in solution by electrospray ionization mass spectrometry. Anal. Chem. 77 (2005) 5370-5379

[46] R.A. Jockusch, P.D. Schnier, W.D. Price, E.F. Strittmatter, P.A. Demirev, E.R. Williams, Effects of charge state on fragmentation pathways, dynamics, and activation energies of ubiquitin ions measured by blackbody infrared radiative dissociation. Anal. Chem. 69 (1997) 1119-1126

[47] Y. Huang, J.M. Triscari, G.C. Tseng, L. Pasa-Tolic, M.S. Lipton, R.D. Smith, V.H. Wysocki, Statistical characterization of the charge state and residue dependence of low-energy CID peptide dissociation patterns. Anal. Chem. 77 (2005) 5800-5813

Table 1. Analysis of results of MD simulations performed on S_4^{16+} ions with five different charge configurations.

Configu-ration	Subunit	Protonated residues[a]	RMSD[b] (Å) (Subunit)	RMSD[c] (Å) (Residues 1 – 21)
16_1	A	N-Ala, Asn11, Arg41, Arg47, Arg72, Lys109, Lys120	4.9 ± 0.2	3.7 ± 0.3
	B	Arg47, Lys109, Lys120	4.9 ± 0.2	
	C	Arg47, Lys109, Lys120	3.8 ± 0.1	
	D	Arg47, Lys109, Lys120	3.7 ± 0.2	
16_2	A	N-Ala, Ala21, Arg41, Arg47, Arg72, Lys109, Lys120	7.4 ± 0.3	9.3 ± 0.5
	B	Arg47, Lys109, Lys120	3.2 ± 0.1	
	C	Arg47, Lys109, Lys120	3.4 ± 0.2	
	D	Arg47, Lys109, Lys120	4.1 ± 0.3	
16_3	A	N-Ala, Tyr31, Arg41, Arg47, Arg72, Lys109, Lys120	15.3 ± 0.7	3.9 ± 0.3
	B	Arg47, Lys109, Lys120	4.6 ± 0.2	
	C	Arg47, Lys109, Lys120	4.0 ± 0.2	
	D	Arg47, Lys109, Lys120	4.0 ± 0.3	
16_4	A	N-Ala, Arg41, Arg47, Arg72, Arg91, Lys109, Lys120	3.3 ± 0.1	2.7 ± 0.2
	B	Arg47, Lys109, Lys120	4.3 ± 0.1	
	C	Arg47, Lys109, Lys120	3.8 ± 0.2	
	D	Arg47, Lys109, Lys120	3.7 ± 0.2	
16_5	A	N-Ala, Arg41, Arg47, Lys120	4.0 ± 0.2	2.8 ± 0.1
	B	N-Ala, Arg41, Arg47, Lys120	5.0 ± 0.2	
	C	N-Ala, Arg41, Arg47, Lys120	4.2 ± 0.3	
	D	N-Ala, Arg41, Arg47, Lys120	4.2 ± 0.2	

a. The residues indicated correspond to the protonation sites in each subunit. All remaining residues are in their neutral form. Residue numbering is based on the truncated form of the core streptavidin used in this study. b. The C_α RMSD was calculated for each subunit with respect to the crystal structure of S_4 with extended N- and C-termini. c. The C_α RMSD was calculated for residues 1 – 21 of subunit A with respect to the crystal structure of S_4 with extended N- and C-termini.

Figure captions

Figure 1. Positive ion ESI mass spectra for a neutral aqueous ammonium acetate (10 mM) solution of S_4 (10 μM) acquired (a) with and (b) without the use of the air flow-assisted nanoESI device.

Figure 2. BIRD mass spectra measured for the S_4^{+16} at the reaction temperature 161 ^oC and reaction times (a) 0 s, (b) 2 s and (c) 5 s.

Figure 3. BIRD mass spectra obtained for the protonated S_4^{+16} ion at (a) reaction temperature 151 ^oC and reaction time 11 s; (b) 141 ^oC and 20 s and (c) 131 ^oC and 40 s.

Figure 4. BIRD mass spectra obtained for the protonated S_4^{+15} ion at (a) reaction temperature 161 ^oC and reaction time 20 s; (b) 151 ^oC and 15 s; (c) 141 ^oC and 28 s and (d) 131 ^oC and 60 s.

Figure 5. BIRD mass spectra obtained for the protonated S_4^{+17} ions at (a) reaction temperature 161 ^oC and reaction time 2.5 s; (b) 151 ^oC and 10 s; (c) 141 ^oC and 16 s and (d) 131 ^oC and 30 s.

Figure 6. (a) Plots of the natural logarithm of the normalized intensity (I/I_o) of the S_4^{+16} ion versus reaction time measured 161^oC (○), 151 ^oC (□),141 ^oC (Δ) and 131 ^oC (◊). (b) Plot of $R_{c/s}$ versus the extent of reactant ion dissociation measured for the S_4^{16+} ion at 161^oC, 151 ^oC and 141 ^oC. The magnitude of $R_{c/s}$ was calculated using the following equation:

$$R_{c/s} = \left(Ab_{(S_3 y_{106})^{+14}} + Ab_{(y_{106})^{+6}} + Ab_{(y_{106})^{+7}} \right) / \left(Ab_{S^{+7}} + Ab_{S^{+8}} + Ab_{S^{+9}} \right).$$

Figure 7. (a) Crystal structure (PDB ID: 1SWB) of S_4 with extended N- and C-termini. Representative snapshots obtained from MD simulations for charge configurations (b) 16_1, (c) 16_2, (d) 16_3, (e)16_4 and (f) 16_5. Subunits A, B, C and D are colored as green, purple, blue and yellow, respectively. The N-terminal region (residues 1 – 21) of subunit A is shown in black.

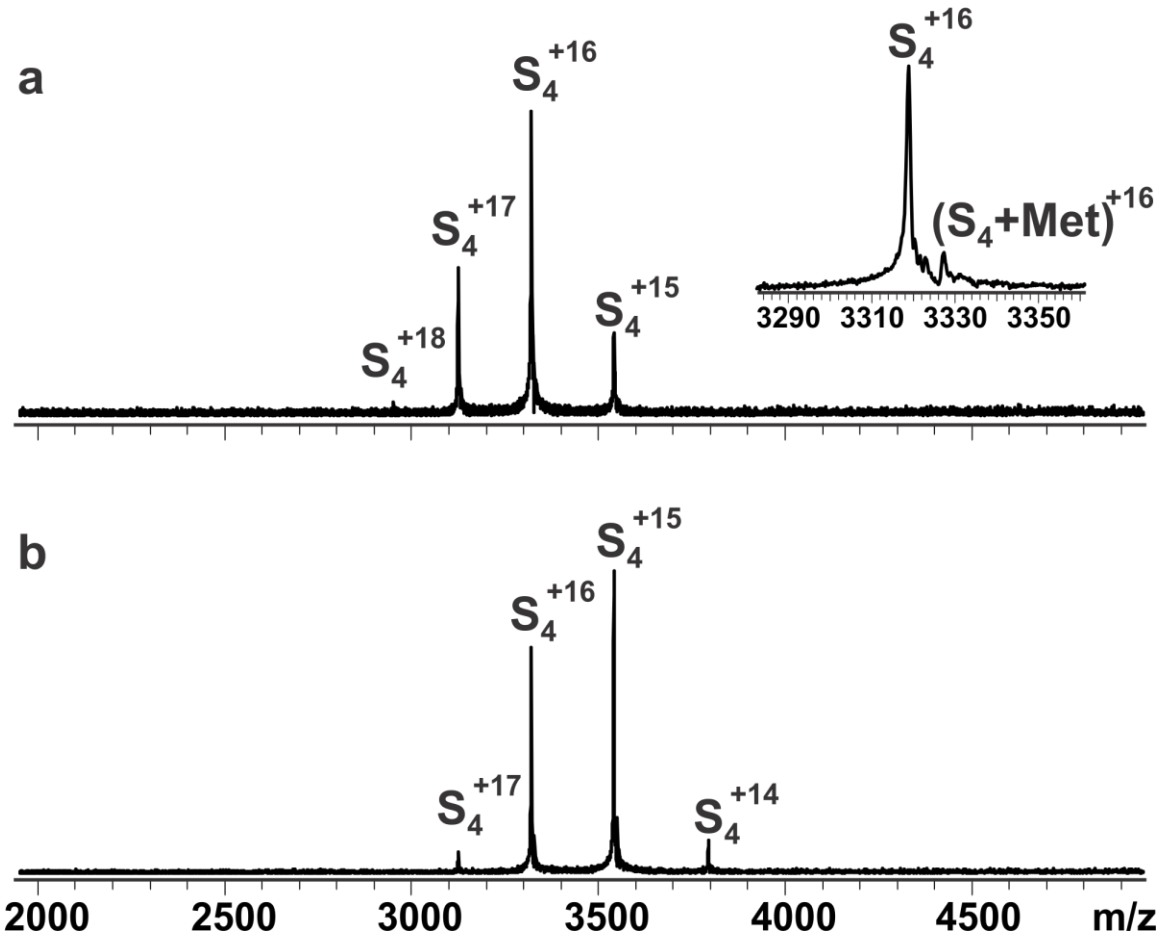
a
S_4^{+16}
S_4^{+17}
S_4^{+18}
S_4^{+15}
S_4^{+16}
$(S_4+Met)^{+16}$
3290 3310 3330 3350
b
S_4^{+15}
S_4^{+16}
S_4^{+17}
S_4^{+14}
2000 2500 3000 3500 4000 4500 m/z

Figure 1

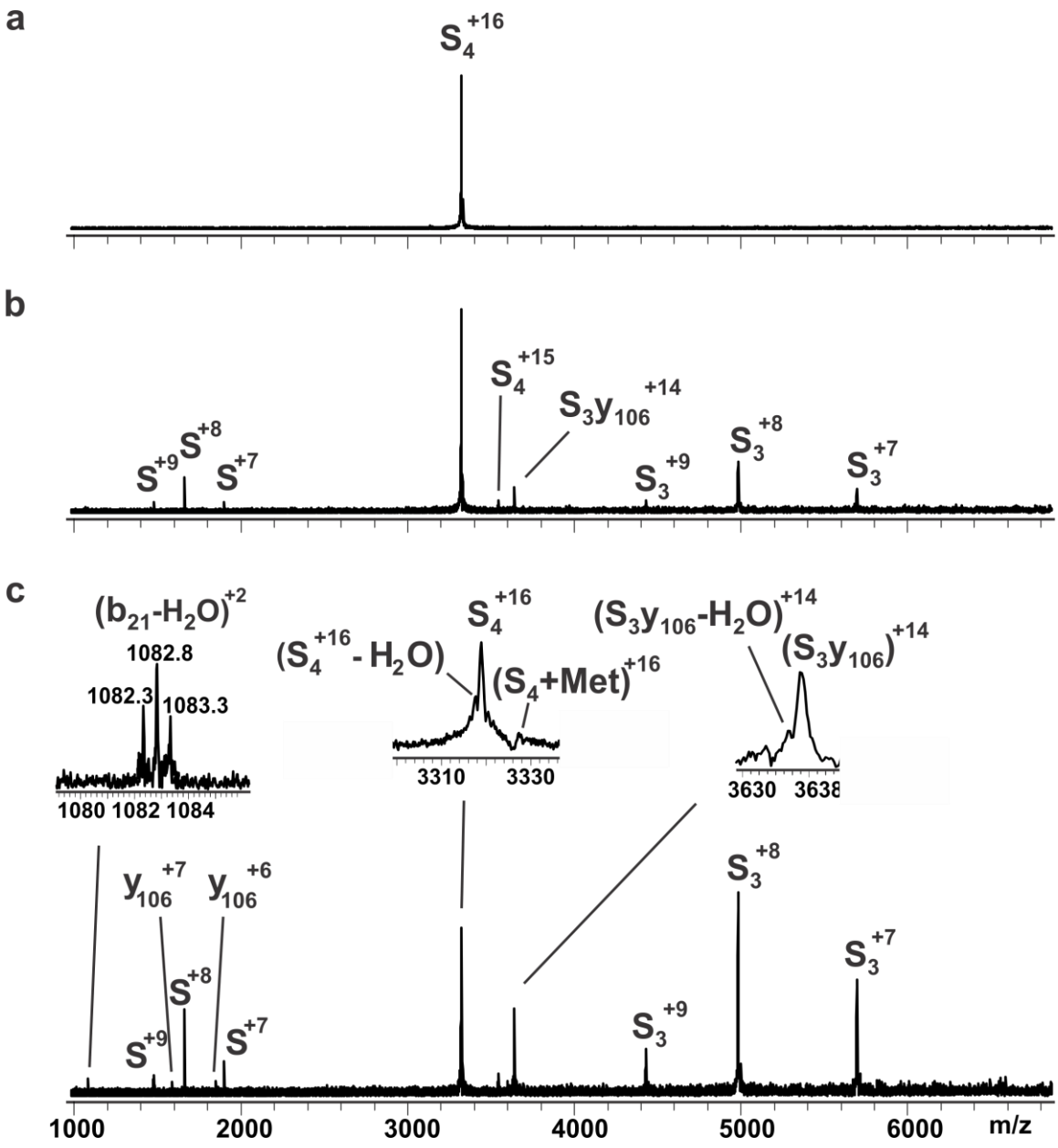
a
S_4^{+16}
b
S^{+9}
S^{+8}
S^{+7}
S_4^{+15}
$S_3y_{106}^{+14}$
S_3^{+9}
S_3^{+8}
S_3^{+7}
c
$(b_{21}\text{-}H_2O)^{+2}$
1082.8
1082.3
1083.3
1080 1082 1084
$(S_4^{+16}\text{- }H_2O)$
S_4^{+16}
$(S_4\text{+Met})^{+16}$
3310 3330
$(S_3y_{106}\text{-}H_2O)^{+14}$
$(S_3y_{106})^{+14}$
3630 3638
y_{106}^{+7}
y_{106}^{+6}
S^{+9}
S^{+8}
S^{+7}
S_3^{+9}
S_3^{+8}
S_3^{+7}
1000 2000 3000 4000 5000 6000 m/z

Figure 2

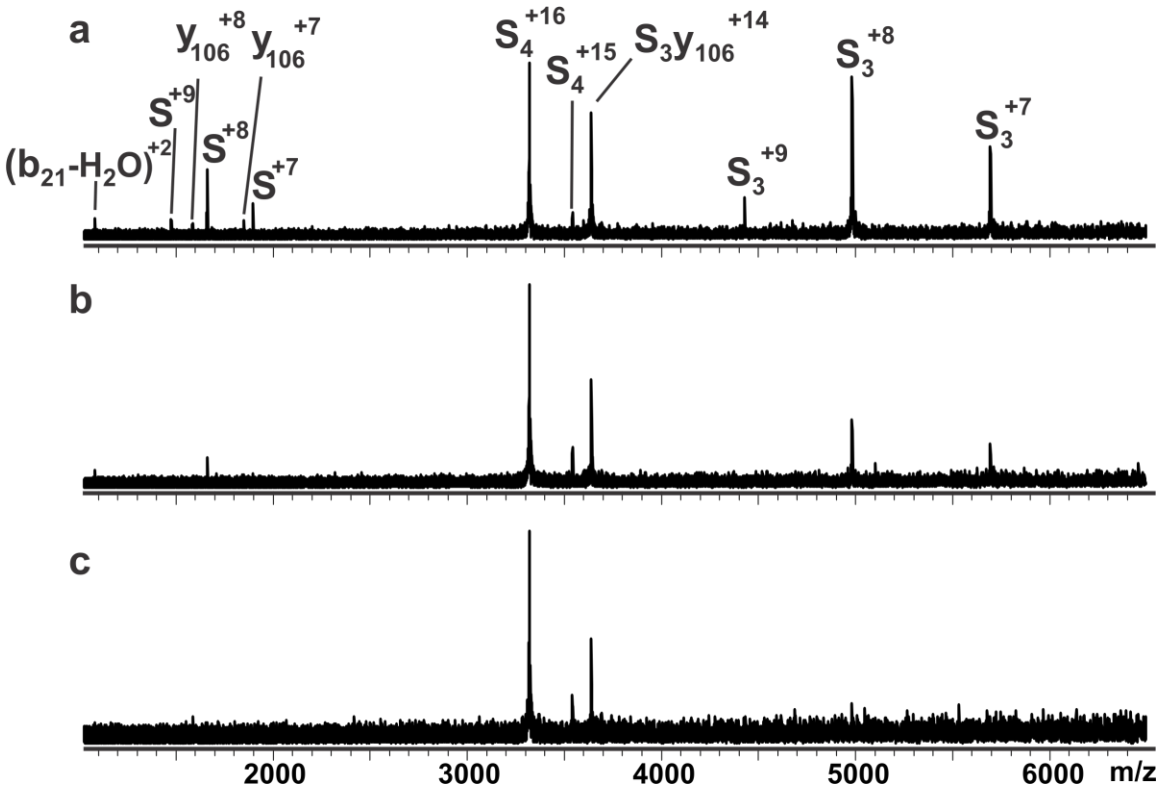
a
b
c
$(b_{21}-H_2O)^{+2}$
S^{+9}
y_{106}^{+8}
S^{+8}
y_{106}^{+7}
S^{+7}
S_4^{+16}
S_4^{+15}
$S_3y_{106}^{+14}$
S_3^{+9}
S_3^{+8}
S_3^{+7}
2000
3000
4000
5000
6000
m/z

Figure 3

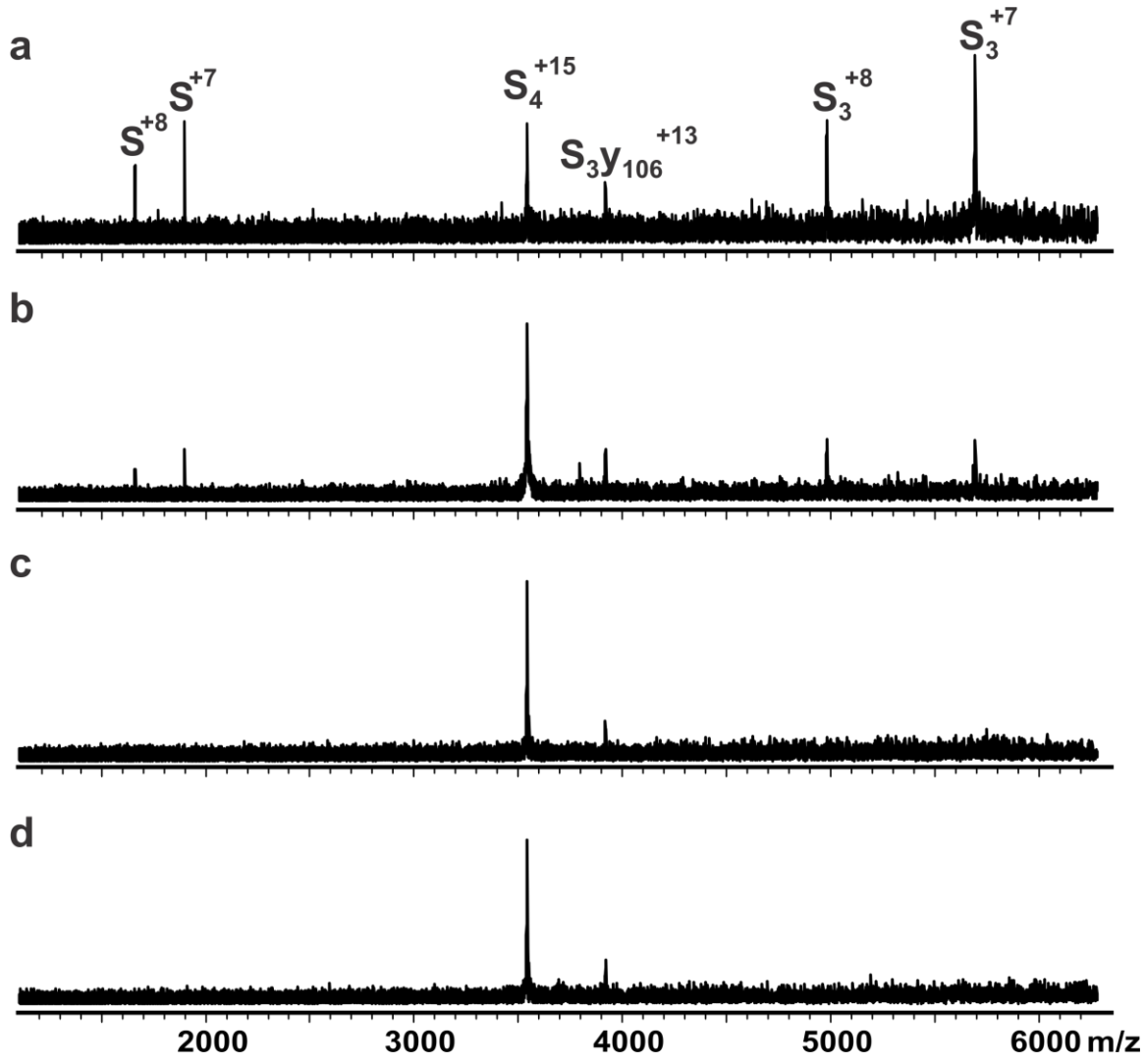

Figure 4

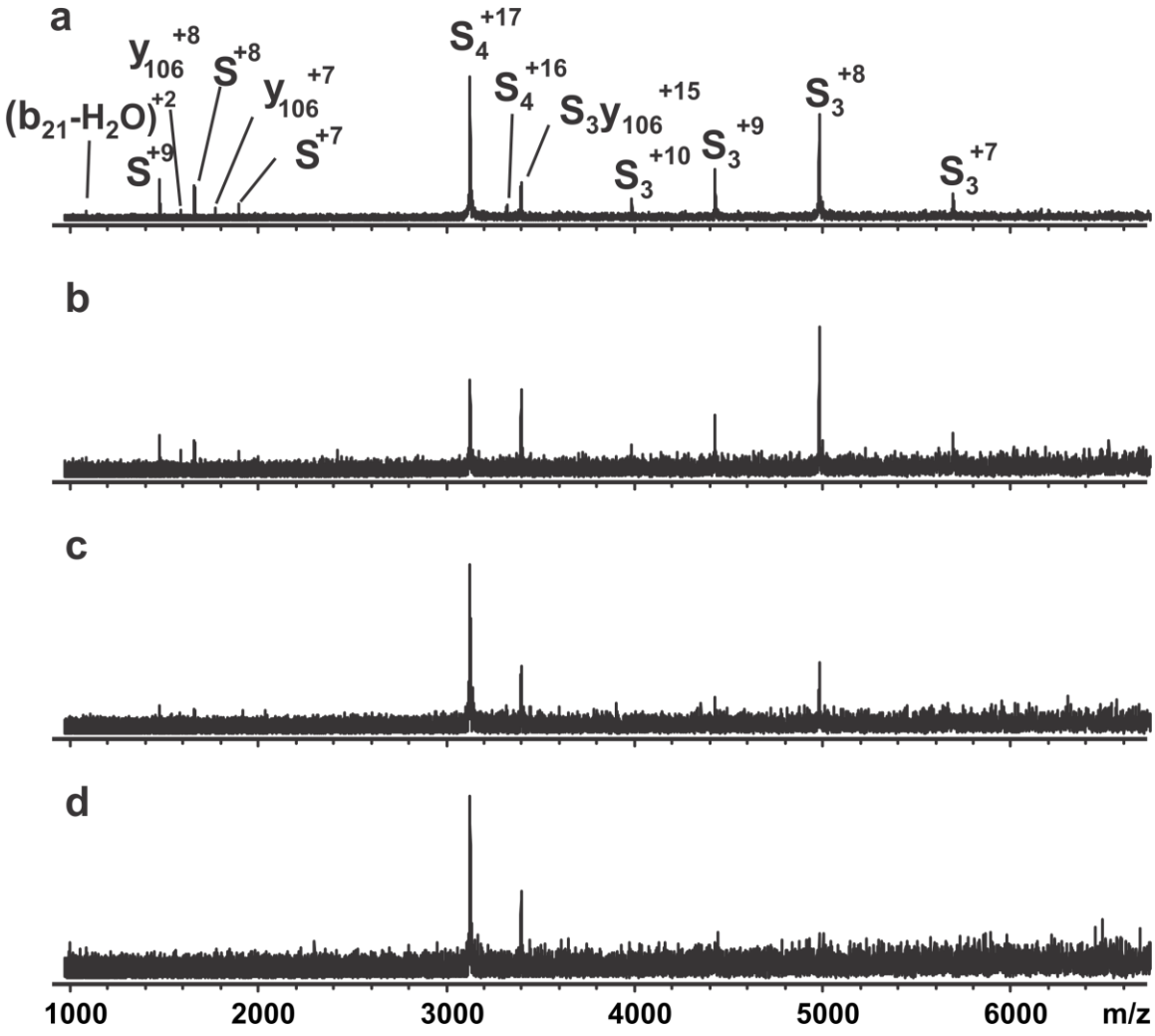
a
b
c
d
$(b_{21}-H_2O)^{+2}$
y_{106}^{+8}
S^{+8}
y_{106}^{+7}
S^{+9}
S^{+7}
S_4^{+17}
S_4^{+16}
$S_3y_{106}^{+15}$
S_3^{+10}
S_3^{+9}
S_3^{+8}
S_3^{+7}
1000
2000
3000
4000
5000
6000
m/z

Figure 5

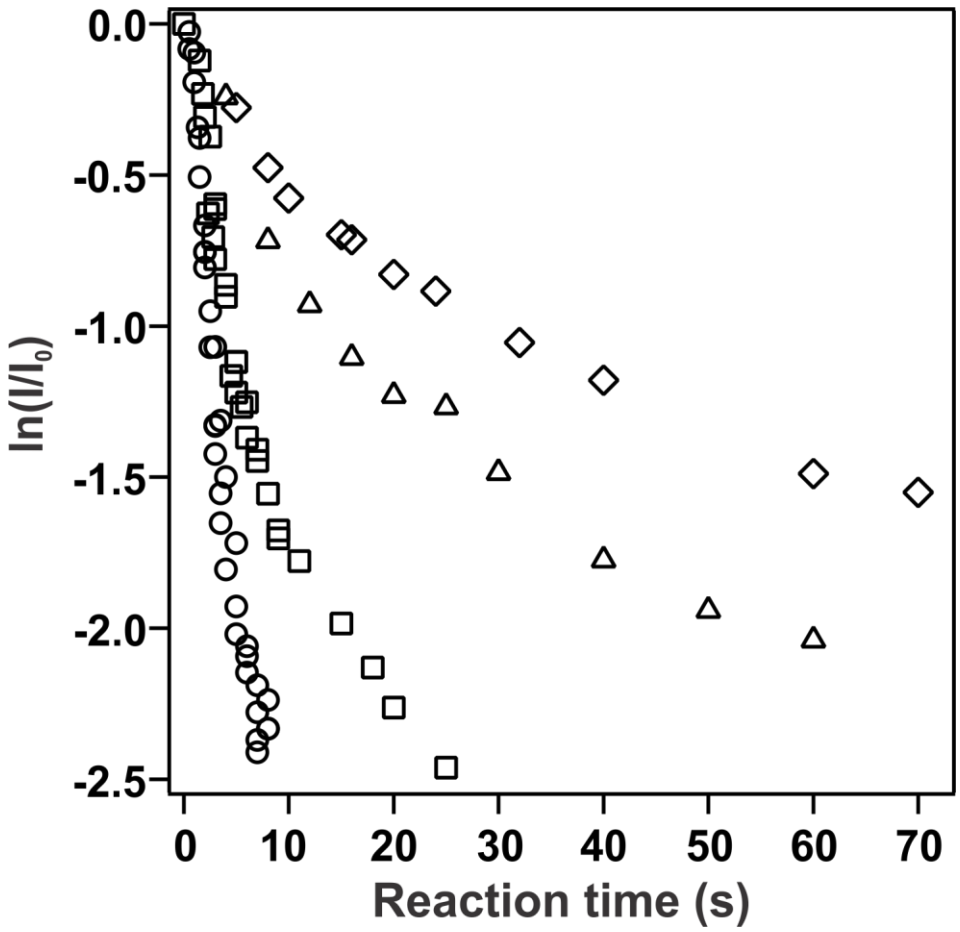

Figure 6a

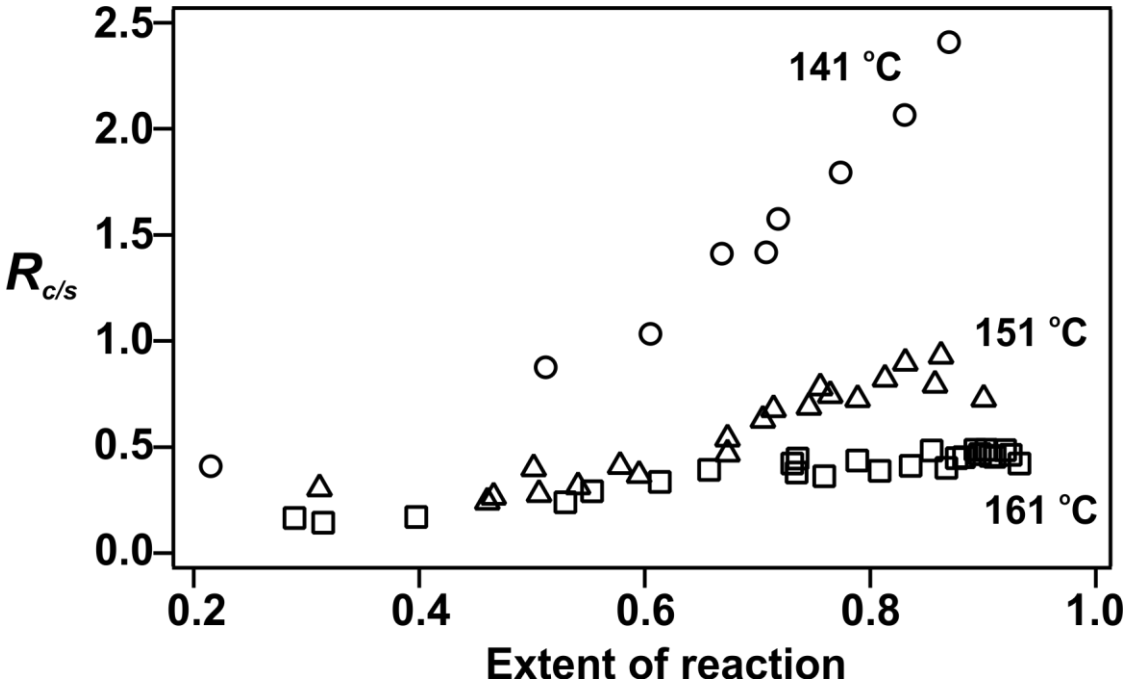
2.5
2.0
1.5
1.0
0.5
0.0
$R_{c/s}$
141 °C
151 °C
161 °C
0.2
0.4
0.6
0.8
1.0
Extent of reaction

Figure 6b

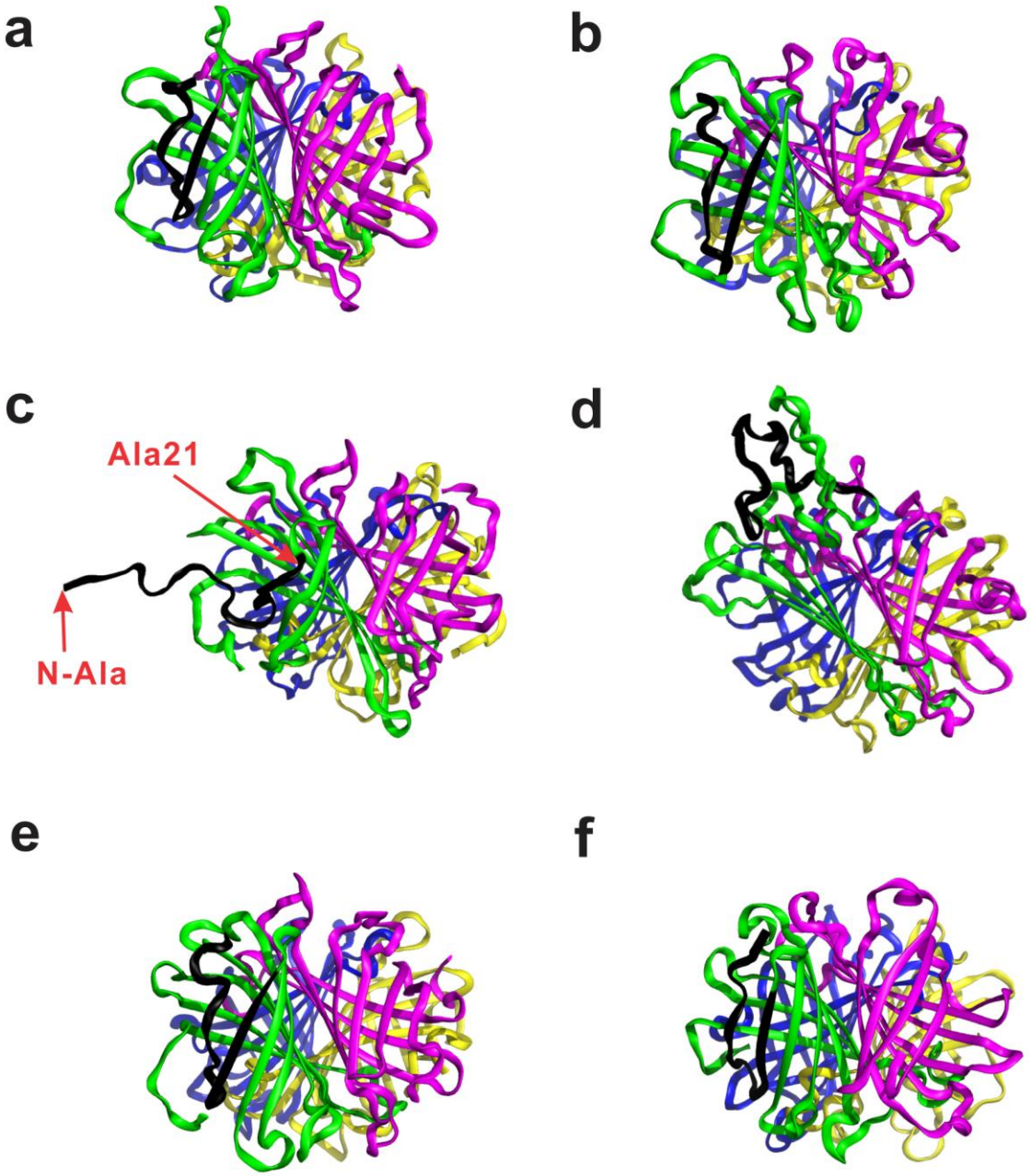

Figure 7